RELATING GLOSS LOSS TO TOPOGRAPHICAL FEATURES OF A PVDF COATING

Jenny Faucheu[1,2], Li-Piin Sung[2], Jonathan W. Martin[2] and Kurt A. Wood[1]

[1] *Atofina Chemicals Inc., King of Prussia PA*
[2] *National Institute of Standards and Technology (NIST), Gaithersburg MD*

Abstract

Semi-gloss commercial poly(vinylidene fluoride) (PVDF) coatings typically have 60° gloss values between 20 and 50. Gloss is affected by PVDF crystallite structures and by the pigmentation. In this paper, we have demonstrated that for some pigmented PVDF coatings after ten years of Florida exposure, the principal proximal cause of gloss changes is the formation of micron-scale pits, rather than the emergence of pigment particles at the coating surface. We have used laser scanning confocal microscopy (LSCM) and light scattering to characterize the surface topography and near-surface structure of weathered and unweathered PVDF coatings. Florida-weathered PVDF coatings show only a modest increase in the root mean square (RMS) roughness of the surface, even when noticeable gloss loss has occurred. LSCM images were analyzed using the Fast Fourier Transform (FFT) and Autocorrelation Function (ACF) techniques. Changes in gloss can be correlated with surface roughness and other topographical features, including the formation of pits and the emergence of pigments.

Introduction

Gloss and color retention are common performance attributes used in the coating industry to measure the weatherability of paints and coatings, particularly decorative coatings used in architectural, automotive, and other applications. As measures of paint performance, gloss and color can be easily and quantitatively assessed. However, the gloss and color measurement scales cannot in general be directly correlated with more fundamental micro-physical surface properties of a material. Thus, when a coating begins to degrade in an outdoor environment, it is not possible to link these optical changes to the chemical and physical molecular or microscopic precursors.

We use laser scanning confocal microscopy (LSCM) and other techniques to probe naturally and artificially weathered PVDF architectural paints. Typical PVDF paint binder compositions consist of 70 % to 80 % (by mass fraction) PVDF resin, and 20 % to 30 % of a miscible acrylic co-resin (e.g. a methyl methacrylate-ethyl acrylate copolymer[1]). For pigmentation, the paints generally use inorganic metal oxides. Coating grade PVDF resin is semi-crystalline with a melting temperature, T_m, of about 165 °C. As the coating is baked above T_m, the resin components form a miscible alloy, and upon cooling, form a film comprised of a complex mixture of crystalline and amorphous regions. The applied paints typically are semi-gloss in aspect (60° gloss values between

about 20 and 50), with surface features influenced both by PVDF crystalline structures and by pigmentation. Thus, there are a number of differences between these paints and automotive coating systems that have been examined in many recent service life prediction studies[2]: PVDF paints are thermoplastic (but semi-crystalline); they are pigmented; and they start with a somewhat rough, semi-gloss surface.

The motivation for this study is to understand how best to track early changes in a thermoplastic paint as it weathers, which ultimately lead to service life failure through gloss loss. Unlike thermoset clear coats, where it is easy to use vibrational spectroscopy to track photochemical changes leading to catastrophic network failure, observable chemical changes in thermoplastic coatings can be more modest, because of mechanisms like surface erosion which remove degraded material from the surface of the sample[3]. By using microscopic techniques like LSCM and atomic force microscopy (AFM), however, the physical changes in the coating can be probed directly. As a first step in this quest to be able to predict weatherability from early tests, in this paper we compare unweathered coatings with moderately weathered coatings—coatings which are just at the half way point for gloss retention, after about 10 years to 12 years Florida exposure.

Experimental[*]

Materials
Paint samples used in this study were model formulations based on commercial PVDF paint formulations, and contained PVDF and acrylic resin blended in a 70:30 mass fraction ratio. A typical formulation contained 24 g coatings grade PVDF (Atofina Chemicals, Inc.), 25 g Paraloid B-44 acrylic (40 % solution in toluene) (Rohm and Haas Company), 16 g weatherable metal oxide pigment, and 35 g isophorone. Pigments used include Shepherd Blue 190 (C.I. Pigment Blue 36, Shepherd Color Company), other mixed metal oxide pigments from the Shepherd Color Company, and TiPure R-960 rutile titanium dioxide (DuPont Corp.). Paints were applied by wire wound rod to chromated aluminum test panels, and baked in a high temperature oven for 45 s, to a peak metal temperature of 254 ºC, then water quenched. Average dry film thickness was 18 μm to 25 μm.

Three coated panels, weathered ten years in Florida, were studied. These panels have been designated as follows:
A: Pigment Shepherd Blue 190, exposed 10 years in Florida.
B: Pigment Shepherd Blue 190, exposed 10 years in Florida.
C: Pigment Shepherd Blue 211, exposed 10 years in Florida.

---

[*] Certain instruments or materials are identified in this paper in order to adequately specify experimental details. In no case does it imply endorsement by NIST or imply that it is necessarily the best product for the experimental procedure.

Weathering
Painted test panels were exposed in Miami, South Florida at 45º south exposure, on open backed racks. On an approximately annual basis, half of the panel was lightly washed with a sponge, then both the washed and unwashed portions were rated for gloss and color. For this study, microscopy work was performed on the unwashed portions of the panels. In some cases unexposed control samples, stored in the laboratory from the same batch as that of the exposed samples, were available for reference.

Laser scanning confocal microscopy (LSCM)

A Zeiss model LSM510 reflection laser scanning confocal microscope (LSCM) was employed to characterize the surface morphology (topographic profile) and to measure the surface roughness of the coatings. LSCM utilizes coherent light and collects light exclusively from the focal plane, while rejecting light out of the focal plane. By using different microscope objectives, the scanned surface area can be varied from 2.6 mm x 2.6 mm down to 20 μm x 20 μm. The incident laser wavelength was 543 nm. The wavelength, numerical aperture (N.A.) of the objective, and the size of the pinhole dictate the resolution in the thickness or axial (z) direction[4]. By moving the focal plane, single images (optical slices) can be combined to build up a three dimensional stack of images that can be digitally processed. Z-steps were selected to obtain overlapping optical slices (a stack of z-scan images). The z-step size was 0.5 μm using objectives of 5x and 10x, and 0.1 μm using objectives of 20x and 150x. LSCM images presented in this paper are 2-D intensity projections (an image formed by summing the stack of images over the z direction, 512 pixel x 512 pixel), or 3-D topographic profiles of the coating surface. The 2-D intensity projection images are effectively the sum of all the light scattered by different layers of the coating, as far into the coating as light is able to penetrate. The pixel intensity level represents the total amount of back-scattered light. Darker areas represent regions scattering less light than lighter colored areas.

From the 3-D topographic profiles, the root mean square (RMS) surface roughness S_q is calculated using a surface tilt correlation (automatic plane fit) without a numerical filter, according to the following formula:

N_x, N_y …number of pixels in X- or Y-direction.

$$S_q = \sqrt{\frac{1}{N_x \cdot N_y} \cdot \sum_{i=1}^{N_x} \sum_{j=1}^{N_y} \cdot \left[z(x_i, y_j) - S_c \right]^2}$$

$$S_c = \frac{1}{N_x \cdot N_y} \cdot \sum_{i=1}^{N_x} \sum_{j=1}^{N_y} \cdot z(x_i, y_j)$$

The estimated uncertainties in the roughness data presented in this paper are at one standard deviation from the mean measurements obtained from at least 6 locations of the same samples. All uncertainties are indicated in the figures as well as in the table.

Gloss measurement
Gloss measurements were made using a handheld commercial glossmeter (Minolta, Multi-Gloss model 268). Measurements conform to the ASTM D 523 standard measurement protocol. For architectural coatings, the 60° gloss measurement is the one

that is most often cited in architectural specifications. The reflectance area for 60° gloss measurements was 9 mm x 18 mm. The collection angular range is ± 0.9° (this angular range is specified by manufacture) from the specular angle. All data presented in this report are the average of 36 measurements obtained from each of 6 different locations (6 measurements per location). The estimated uncertainties in the gloss measurement presented in this paper are at one standard deviation from the mean value for all 36 measurements.

Light scattering
To ascertain the specular and non-specular scattering distribution from the coating and the substrate surfaces, light scattering measurements were performed on both exposed and unexposed sections of the PVDF paint samples, using a newly constructed light scattering instrument located in the NIST Building and Fire Research Laboratory. The new instrument consists of a laser light source, a five-axis goniometric sample stage, and a two-dimensional detector mounted in a concentric ring around the sample stage. The incident laser wavelength was 633 nm, and the beam was polarized and focused on the sample with a diameter of 1 mm. The sample rotation stage and the detector ring position determine the incident angle of the beam on the sample and the viewing angle of the detector. Figure 1 presents the optical geometry, where θ_o and θ_s are the incidence and scattering angles measured with respect to the normal of the sample. The sign convention is such that $\theta_s = -\theta_o$ indicates the specular reflection angle. A detailed description of the instrument will be reported elsewhere[5]. In this study, we present the results in terms of the two-dimensional angular distribution of light scattered from a coating surface at incident angle of 60°. The results were compared to gloss and the LSCM results. The estimated uncertainties in the light scattering intensity data are to be around 4 %.
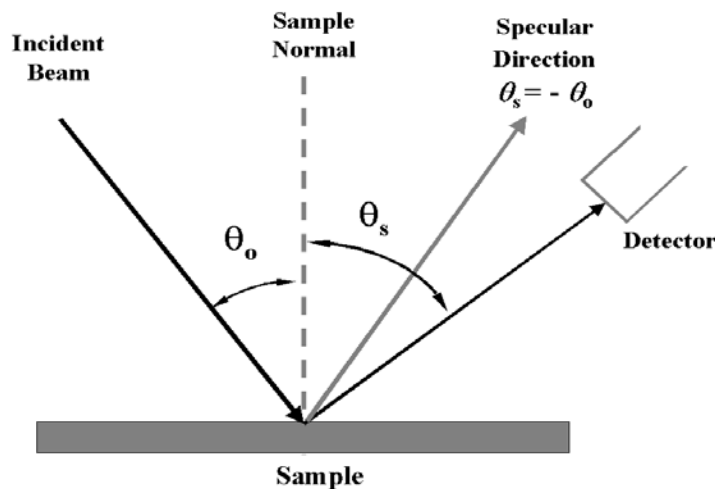

Figure 1. Geometry for the incident and scattering angles.

Results and Discussion

Effects of weathering

Using the techniques described above, a number of PVDF coatings, exposed in Florida for 10 years, were examined and compared against either control samples that were prepared at the same time as the samples that were exposed, or against the masked area of the exposed panels. For the exposed panels, some loss of coating gloss was visible to the naked eye at certain angles—however, as seen in Figure 2, the color change in these coatings is typically small. The typical gloss retention for masstone coatings was about 50 % after 10 years' exposure in Florida. For coating #A, the gloss of the masked area was 48, and the gloss of the exposed area was 21.
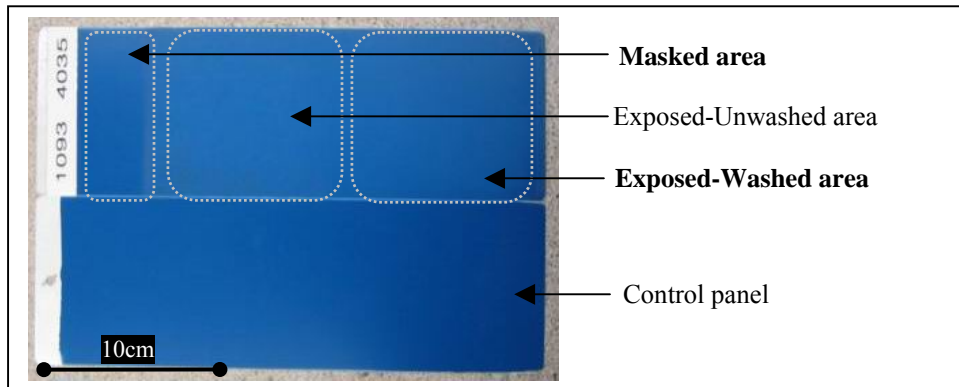

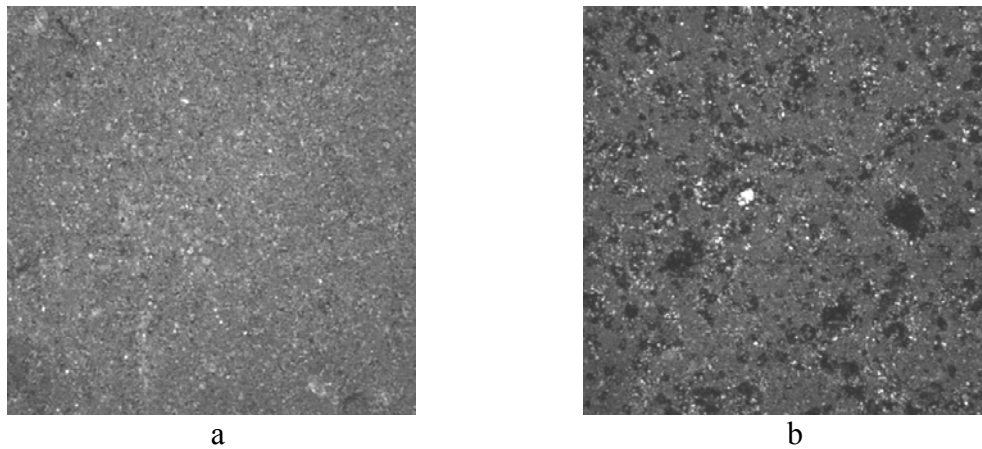*Figure 2. Coated panel exposed in Florida (Coating #A) and Control panel.*

a   b

Figure 3. LSCM 2-D projection images (150x magnification-61.4μm x 61.4 μm) of Coating #A obtained from (a) masked area: RMS roughness 0.15 μm, Gloss 48, and (b) exposed areas: RMS roughness 0.27 μm, Gloss 21.

Changes in the coating surface topography after exposure were evident at the microscopic level, as shown in the 2-D intensity projection images in Figure 3a-b. Figure 3a shows the masked area, while Figure 3b shows the exposed area.

In the masked area (Figure 3a), the binder (gray background) appears to be homogeneous – the deviations in the height and intensity profiles are small. A few white spots are also visible in Figure 3a. For the exposed area (Figure 3b), the overall intensity of the white spots appears to be higher than in Figure 3a, while the number of white spots appears to increase slightly. A detailed discussion of the differences in the scattered intensity distribution between the masked and exposed areas is presented below. However, from a comparison of different coating systems, it is clear that the white spots represent pigment particles on or near the top surface, which scatter more light than the binder. According to the pigment product literature, the average size of the pigment particles for coating #A is around 0.8 μm. In the LSCM images, the size of the white spots is much less than 0.8 μm in height as well in length – presumably because much of the pigment particle remains embedded in the binder. AFM measurements were also performed to examine the topographic feature of the white spots, and gave similar results. At a magnification of 150x, the LSCM RMS roughness was $S_q = 0.15$ μm for the masked area.

Unlike the image of the masked area, the 2-D intensity projection images of the exposed area also show many dark regions. The dark regions are associated with depressions or pits in the coating, as illustrated in the height profile of these areas (Figure 4). Typical sizes for the pits are 1 μm to 4 μm in length (x-y directions) and 1 μm to 2 μm in depth (z-direction). The surface roughness increases due to the height variation associated with pit formation—an RMS roughness $S_q = 0.27$ μm was obtained from the exposed area. Figure 5 shows the intensity profile from representative topographic features (binder, pit, pigment) in the Figure 3b image. For this particular coating, after 10 years' of exposure in Florida, the increase in the surface roughness and the decrease in coating gloss both appear to be dominated by pit formation as opposite to ablation of the coatings and consequential emergence of pigment particles.
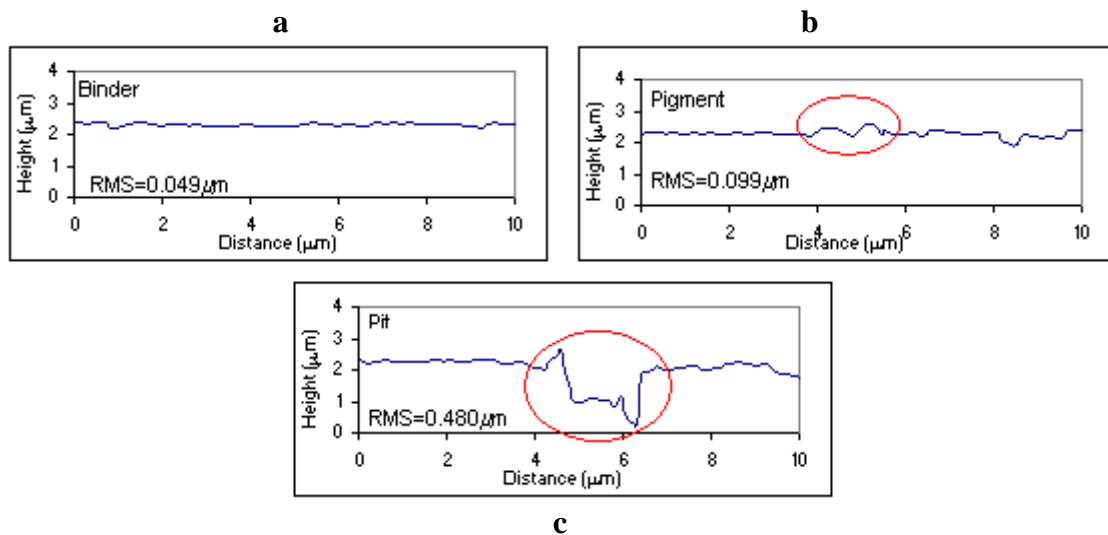

Figure 4. LCSM height profile (**a**) gray area (binder), (**b**) bright area (pigment), and (**c**) dark area (pits) obtained from Figure 3b image.
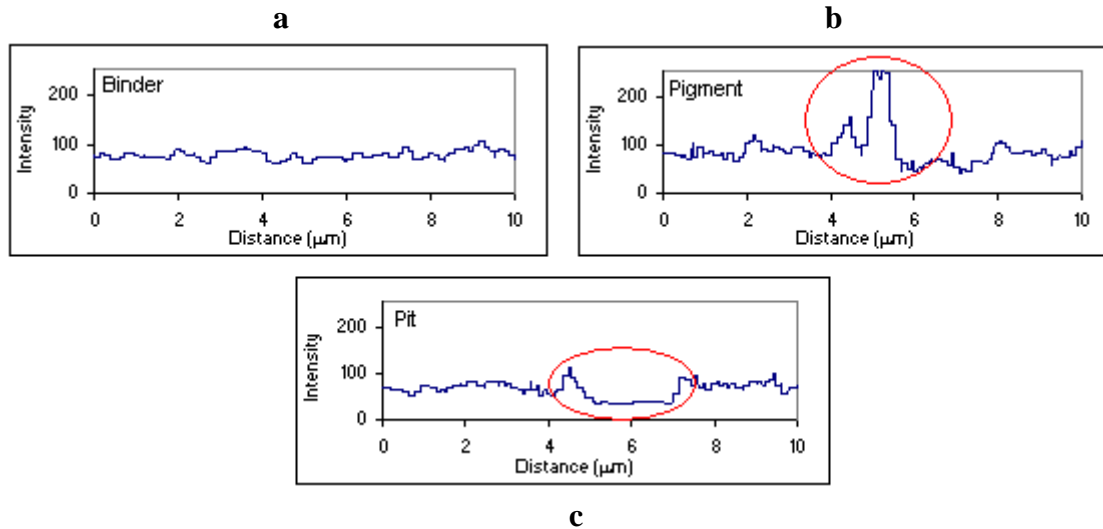
*Figure 5. LSCM intensity profile – (**a**) Binder – (**b**) Pigment – (**c**) Pit, obtained from Figure 3b image.*

Visually comparing the LSCM images for about a dozen weathered PVDF coatings, there generally appears to be an increase in the pigment density at the coating surface after weathering. Such an increase would be consistent with general models of erosion or contraction of pigmented coatings[6,7], which link gloss loss to the emergence of pigment particles at the coating surface. However, the visual comparisons are based on a subjective assessment of the intensity of the white spots in the image, and tend to confound areal density and scattering intensity effects. Many of the weathered coatings also show evidence of depressions or pits in the coating, at a 1 μm to 4 μm length scale. However, it should be noted that pits or depressions are not observed in all PVDF coatings with this same degree of weathering. In comparing a series of coatings made with different single mixed metal oxide pigments, depressions are evident for some of the coatings, but not for others. The reasons for this difference are not understood. In the current study, we have chosen to conduct most of our analysis on coatings with pits, since this kind of surface feature, at this scale, has received little if any attention to date in studies of pigmented coatings, (a number of recent AFM studies[8,9] have reported smaller depressions or pits in studies of clear coats).

Comparison between surface roughness and gloss

Since most of the light reflected in gloss measurements is reflected off of the top surface of the sample, we analyzed a number of weathered and unweathered PVDF paints to determine the degree of correlation between the gloss of the coatings and simple measures of the surface topography such as the RMS (root mean square) roughness. LSCM and gloss measurements were conducted on 14 exposed coatings (exposed and masked areas), and 25 unexposed coatings (control). The exposed coatings had a variety of different weathered coating morphologies (some with pits, some without). To evaluate the variability of the measurement procedure, multiple measurements were performed on four of these coatings. Comparisons of gloss values and RMS surface roughness are shown in Figure 6, for different LSCM magnification scales: 5 x and 150x.
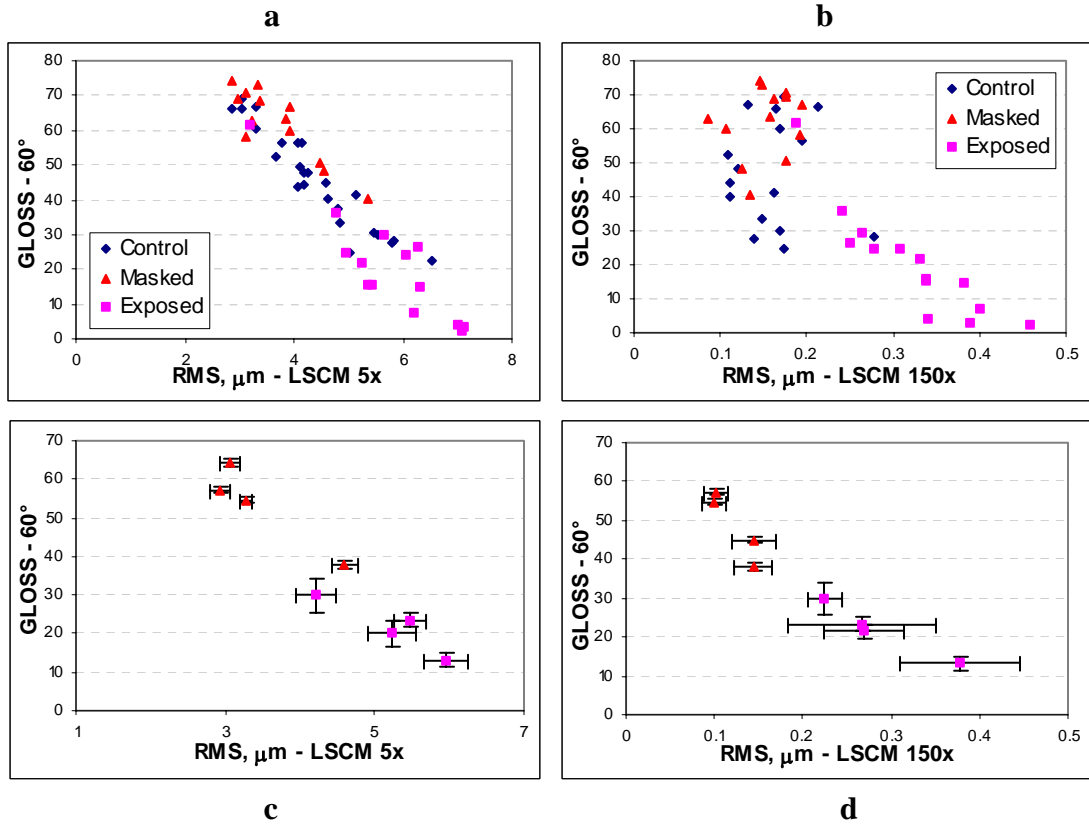
*Figure 6. Gloss vs. RMS surface roughness obtained from (**a**) LSCM-5x (**b**) LSCM-150x measurements for 14 different coatings, exposed and masked areas, and 25 unexposed coatings, one RMS roughness measurement and six gloss measurements per point. The estimated extended uncertainties (k=2, 2σ) of (**c**) LSCM-5x and (**d**) LSCM-150x for four different coatings, exposed and masked areas, six locations per point (six gloss measurements and one RMS roughness measurement per location).*

The different LSCM magnification levels probe different length scales of the coating surface, as are seen in the abscissa scales of the above plots of the RMS roughness. Typical RMS roughness levels are in the micrometer range using 5x-magnification, but are ten times smaller at 150x-magnification.

Figure 6a and 6c show that at the 5x-magnification scale, the reproducibility of the RMS roughness measurement is good, and for these different PVDF based coatings, a reasonably good correlation of gloss and RMS roughness is obtained[10] ($R^2 = 0.90$, where R is the goodness of the fit). Similar results were obtained at 20x magnification. However, at 150x-magnification, there is a much lower degree of correlation, and the reproducibility of the RMS measurements is relatively poor, especially for the exposed areas. Biggs *et al*. have made a similar observation[11] in an AFM study of the weathering of polyester/melamine paint surfaces. They found limited correlation between RMS evolution and gloss loss in the QUV-B experiments, and little correlation between the relative initial RMS evolution rates, when comparing different accelerated weathering techniques.

These findings illustrate that while high magnification images are very helpful to visualize physical damage in weathered coatings (e.g. the 150x images of Figure 3, or on an even finer scale, scanning electron microscope[12] or AFM images[13]), the coarser, longer wavelength surface roughness most directly relate to the gloss measurement, and to the visual perception of gloss. This result is in line with theoretical expectations[14,15].

For selected cases, the RMS roughness was also measured on a smaller length scale using an AFM. Table I shows the values obtained for panel #B, one of the samples which exhibits pits in the exposed portion of the sample, over a range of length scales from 10 μm to nearly 2 mm:

*Table I. RMS roughness (panel #**B**) on different length scales using AFM and LSCM.*

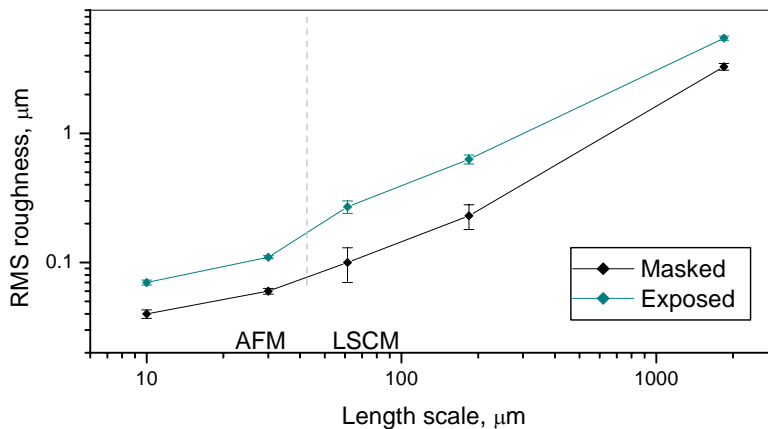|		AFM		LSCM		
Scan size [μm^2]		10x10	30x30	61.4x61.4	184x184	1842x1842
RMS	Masked	0.04	0.06	0.10	0.23	3.28
[μm]	Exposed	0.07	0.11	0.27	0.63	5.47

Figure 7. RMS roughness vs. measured length scale in a double logarithmic plot.

Figure 7 shows there is an almost linear dependence of the RMS roughness with the length scale of the measurement in a double logarithmic scale, i.e. RMS ~ (length scale)^f. This result implies that there is an intrinsic fractal dimension of samples with a local RMS roughness value reflecting structural characteristics at the corresponding measured length scale. In this case, the scaling factor f = 0.983 ± 0.078 for the masked area and f = 0.928 ± 0.039 for the exposed area. Assender *et al.*[16] and Johnson et al.[17] have observed similar results in other coating systems. Moreover, Johnson et al. have identified the scaling region and roughness exponents for different exposure times for a polyurethane system, and also observed that the scaling factor decreased with increasing exposure time. Although it is too early to make any conclusion, fractal analysis may provide a link

between local physical changes in nanoscale to macroscopic measurements, which can be used to predict gloss changes.

Standardization of LSCM 2-D intensity projection images
Since the intensity of the LSCM images is affected by factors such as optical alignment and detector gain, pixel intensity level analyses were conducted for selected images. For the Panel #B images, Figure 8 shows histograms of the number of pixels in each image at each detector intensity level - from 30 (Black) to 255 (white). Note that in this case the lower intensity threshold was set by the signal amplitude and detector gain of LSCM instrument. Each of these histogram curves is the average for six different LSCM images of six different locations on the coating, obtained at the same time with the same detector gain.
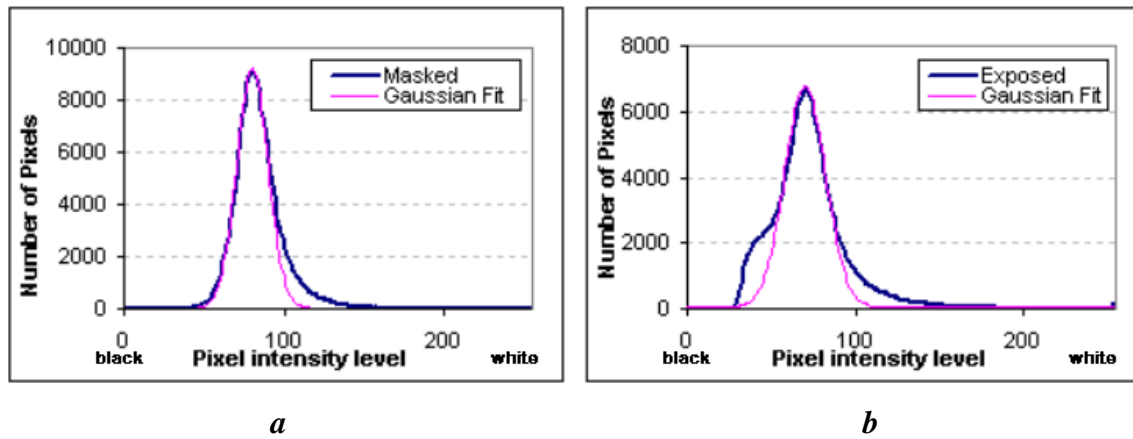

a   *b*

Figure 8. Histogram of the number of pixels in each image (Figure 3) for each pixel intensity level.

The left part of each curve represents the fraction of the surface image that is black or dark gray, darker than the average — areas which correspond to surface depressions (see topographic scans, Figure 4). Comparison of the masked and exposed curves shows clearly that these depressions appear after exposure.

The right part of each curve represents the fraction of the surface image that is brighter than the average, due to the reflectivity of pigment particles at or near the top surface of the paint. The pigment particles appear as white spots because they scatter more light than the binder (Figure 5). The pigment particles near the surface of binder also have an effect on reflected light. The light scattered from these pigments goes through the layer of binder and is added to the light scattered from the top surface of the binder.

To obtain a more quantitative analysis of the distribution of pits and surface pigments in the 2-D projection images, the large central peak in the pixel intensity histograms- due to the principal surface reflection- was modeled as a Gaussian curve. While it is common to use a Gaussian function to model the topographic profile of a rough surface, with the width of the Gaussian distribution being proportional to the RMS of the surface[18], we are not aware of any special theoretical reason why a Gaussian fit would be the most appropriate in this case, where the scattering intensity is being modeled. Nevertheless it

can be noted from Figure 8a that the gray level intensity distribution for the unweathered coating fits the Gaussian form well on the low intensity side (where pigment contributions to the scattering are not important). The parameters obtained for the curves shown (Table II) are:

Table II. Parameters obtained for the curves above (Figure 8).

	Masked	**Exposed**
Pixel intensity level at maximum	80	70
Full width at half height 2w	24	30
Pixel intensity level range at half height	68 to 92	55 to 85

The Gaussian curve can be considered as the intensity distribution expected for binder surface reflections, without any contribution from pigment particles or pits. The difference between the experimental curve and the Gaussian fit reflects the contribution of pigments and pit areas in the total 2-D projection image. Figure 9 shows difference curves for the data of Figure 8. The peaks at intensity level 80 to 150 show the excess number of higher intensity pixels, from locations where surface pigments are present. The additional peak at intensity level 40 to 50, for the exposed sample, shows the excess number of darker pixels in the image, from pit areas. From these curves, the areal contributions of the depressions and the pigments can be calculated directly.
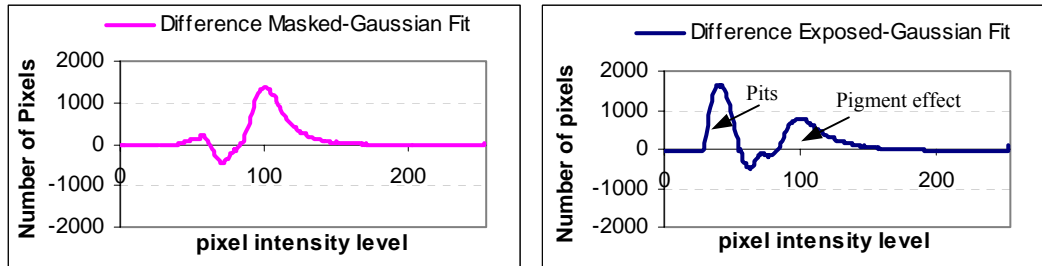

Figure 9. Difference between the real pixel level distribution curve and the Gaussian fit.

Alternatively, the Gaussian fit information can be used to set threshold intensity levels for particular features of the image, to highlight particular topographic components of the surface, so that their distribution can be analyzed using various image analysis methods. Threshold levels should be set individually for each image, since the position and width of the central curve Gaussian fit depends on various LSCM instrumental factors. Using this approach, we have attempted to model the LSCM images of these coatings using four components: Pits – Binder - Binder with sub-surface pigments effect - Top-surface pigment. Each of these components has a different light scattering behavior.

In assigning ranges of pixel intensity levels to each component of the coating, the full width at half-maximum (FWHM), *w,* of the Gaussian fit is chosen as a characteristic parameter to describe the distribution (Figure 10). The Gaussian fit region was considered to reflect the scattering contribution of the binder. Then using the difference curves (Figure 9), top surface pigment contributions were defined to be those excess

pixels (in the ▬ region) with an intensity at least *2.5w* greater than the central peak maximum. Excess pixels (in the ▧ region) with an intensity level between *0.5w* and *2.5w* greater than the central peak maximum were assigned to subsurface pigment particles. Excess pixels (in the ▨ region) with intensity level less than - *0.5w* below the maximum were assigned to pits.
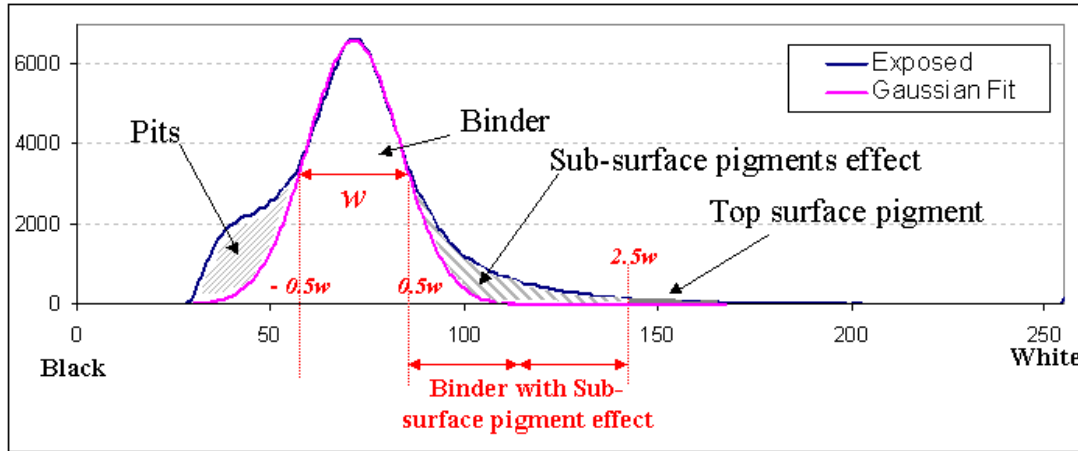

Figure 10. Assignment of each area of the curve to one component of the coating.

The results of this analysis, for Florida panels #A, #B and #C, are shown below as a percentage of the total area (Table III).

Table III. Percentage (the estimated uncertainty is 3 % (one standard deviation)) of the total area$^{\phi}$ covered by each component.

		Pits	Binder	Sub-surface pigment	Top-surface pigment
Masked	#A	0	92	7.5	0.5
	#B	0	89.5	10	0.5
	#C	0	87.5	12	0.5
Exposed	#A	13	75	10.5	1.5
	#B	14	72	11	3
	#C	8	82	8.5	1.5

This analysis shows a significant increase in the area occupied by pits in the exposed coating, and a minimal increase in the density pigment particles on top surface. For these coatings, the changes in the surface pigment density due to exposure are suggestive of some emergence of pigment particles, but the numerical differences are not statistically significant.

To our knowledge, this is the first time that pits of these dimensions have been implicated as the principal proximal cause of gloss changes in some pigmented coatings. The

---

$^{\phi}$ The total area is given by the sum of the Gaussian curve area, the pits area and the pigment effects area.

"contraction" model of Colling and Dunderdale, which is based on the idea of coating binder mass loss not only at the surface, but as far into the coating as photons can penetrate, predicts that inhomogeneous distributions of pigment particles should lead to the generation of pit structures of the type observed. This mechanism could be operative in commercial type PVDF paints, especially since they contain an acrylic component that is less inherently weatherable than the PVDF resin, which could photooxidize leading to binder contraction which is inhomogeneous in the *x-y* plane. To test this hypothesis, we are planning experiments to compare the degree of dispersion of the pigments in the test coatings.

The Gaussian fit threshold criteria were used to create enhanced binary (black and white) images of either the pits (dark areas) or the pigments (bright areas), for further digital analysis using Fast Fourier Transform (FFT) and Autocorrelation Function (ACF) techniques. Figure 11 shows the images obtained, for the panel #B masked and exposed areas. Since the evolution of the surface and near-surface pigment distribution is not dramatic, we have chosen to focus most of our attention on the analysis of the pit distribution.
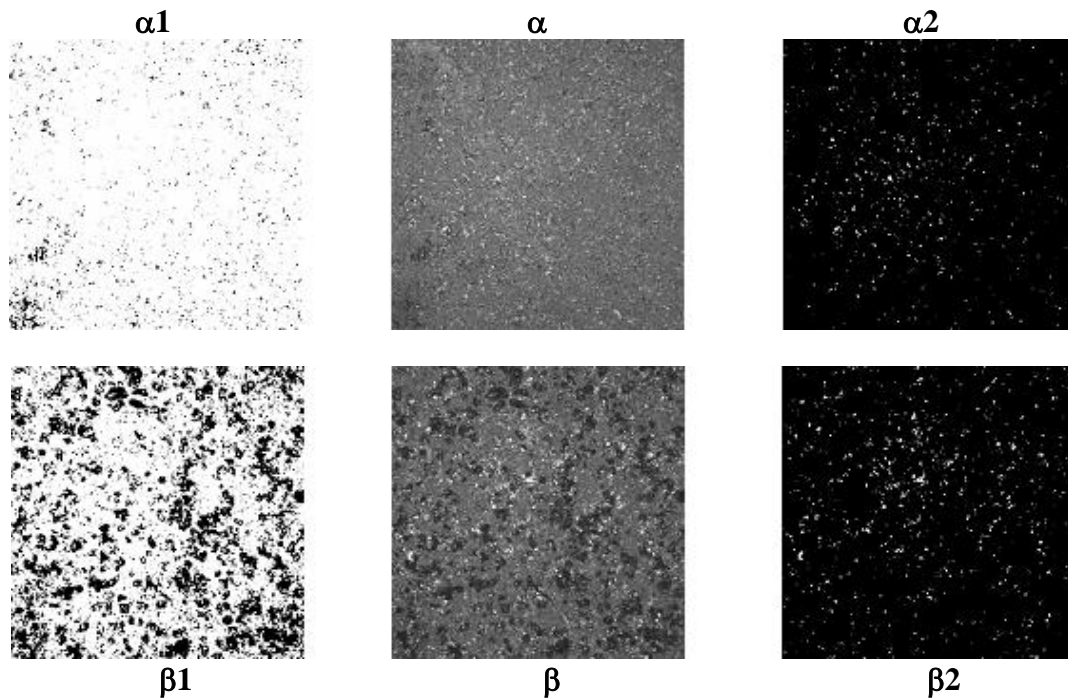

*Figure 11. The images (α) and (β) in the center column are the LSCM projection image obtained from masked and exposed areas of coating **#B**, respectively. Image size is 61.4 μm x 61.4 μm. Images ($\alpha 1$) and ($\beta 1$) in the left column are threshold images of (α) and (β) showing the dark areas (pits) after applying threshold level of 83 and 74, respectively. Images ($\alpha 2$) and ($\beta 2$) in the right column are threshold images showing the bright areas (pigments on top-surface) after applying a threshold level of 172 and 156, respectively.*

Fast Fourier Transform analysis of LSCM images

Figure 12 shows the result of applying a Fast Fourier Transform (FFT) to the pit and pigment threshold images. The result of the FFT of the image is drawn in a Log-Log plot. The real size scale is directly given on the x-axis.
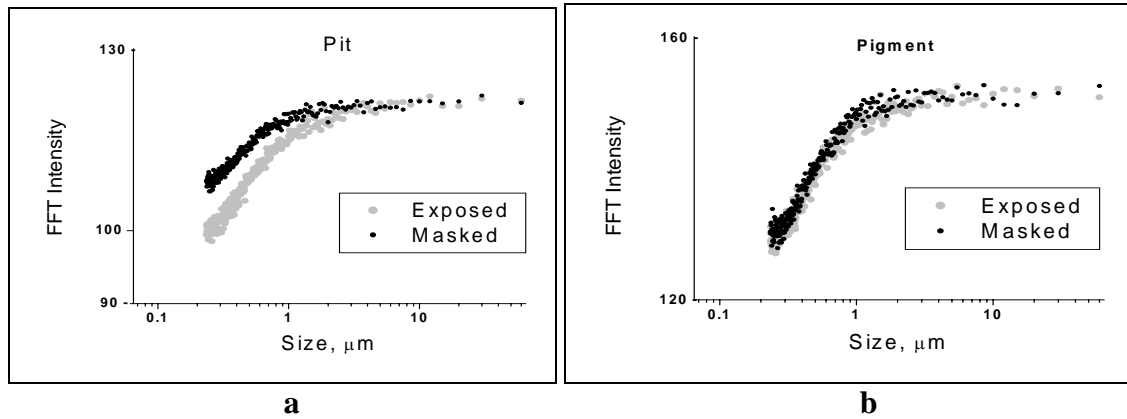

a   **b**

*Figure 12. (**a**) FFT of images α1 and β1, and (**b**) FFT of images α2 and β2. Note: The FFT intensity of each sample has been shifted by a y-axis-translation to be on the same baseline. The x-axis translates directly the real spatial domain.*

Figure 12a shows the FFT curve of the pit regions. The curve corresponding to the exposed coating is shifted to the right. This means that the characteristic length of the pits/darker image regions in the exposed area is larger than the characteristic length of these regions in the masked area. This can easily be seen visually, comparing images α1 and β1 of Figure 11.

However, considering the pigment images, the FFT curves for the masked and exposed area (Figure 12b) are not distinguishable. Thus, the FFT analysis is not appropriate for characterizing the changes in the pigment scattering image—changes which are primarily changes in intensity rather than spatial distribution (images α2 and β2 of Figure 11).
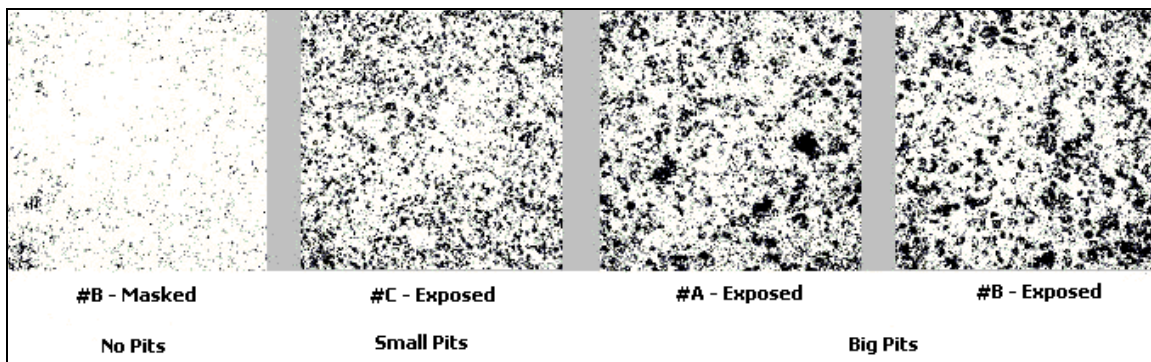

Figure 13. Dark region images of different weathered coatings, using the Gaussian threshold criterion, presenting different sizes and distributions of pits.
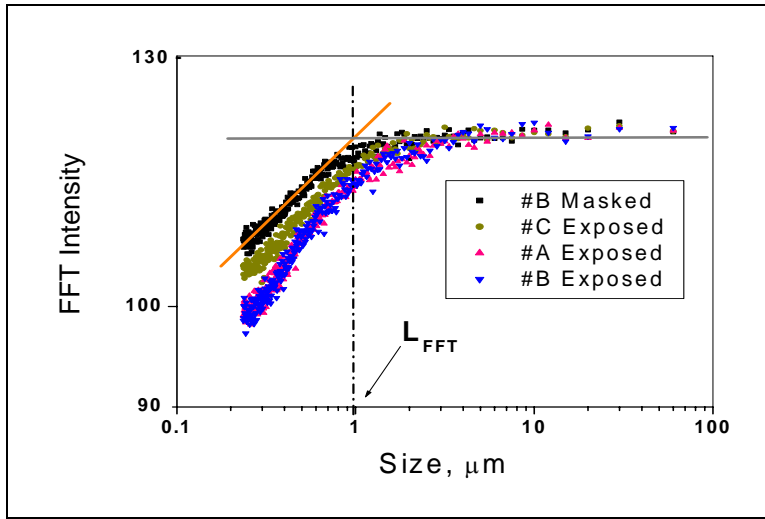
Figure 14. FFTs of the pit distribution images shown in Figure 13.

Figure 13 shows dark region (pit) images obtained from different exposed samples, plus one control: Sample #B-masked, Sample #C-exposed, Sample #A-exposed, and Sample #B-exposed. Figure 14 compares the FFT curves for these images. To obtain a better comparison, a characteristic length L_{FFT} is defined as the location of the "knee" in the curve (in a Log-Log plot). The values of L_{FFT} were estimated and listed in Table IV The results of the FFT analysis can be summarized as follows:

- Sample #A-Exposed and #B-Exposed present the same degradation (same size, same amount of pits), and the FFT of the threshold image gives the same result.
- Sample #C-Exposed presents smaller pits, the curve is shifted to the left compared to #A-Exposed and #B-Exposed, i.e. to smaller characteristic length.
- Sample #B-Masked is a masked area, it presents small dark features. Curve is shifted to the left compared to #C-Exposed, i.e. to even smaller length.

Table IV. Characteristic length from FFT for the four threshold images, and the corresponding gloss values.

	#B-Masked	#C-Exposed	#A-Exposed	#B-Exposed
Characteristic Length L_{FFT} , µm (± 5%)	1.00	1.35	1.46	1.45
60° gloss (±1)	55	30	21	23

As seen in Table IV the larger the L_{FFT}, the lower are the gloss values. This result is consistent with the observation that micron scale structures will be effective in increasing RMS surface roughness, and decrease gloss values, in the exposed coatings. From these examples, it can be seen that an FFT analysis of LSCM images can be used to quantitatively describe the emergence of micron-scale pits on the coating surface.

However, like the RMS roughness analysis, this method may not be sensitive enough to be used in the early prediction of coating gloss retention.

Autocorrelation Function[19] analysis of LSCM images.

Some papers show that the use of autocorrelation functions (ACF) is preferred when studying "random systems". Contrary to FFT, this technique always remains in the spatial domain. For the same four images showing pits (black areas), the two-point correlation functions are determined using the following equation for an M×N pixels image:

$$S(x, y) = \sum_{i=1}^{M-x} \sum_{j=1}^{N-y} \frac{I(i, j)I(x+i, y-i)}{(M-x)(N-y)},$$

where *I(i,j)=1* if the pixel at location *(i,j)* is black and *I(i,j)=0* otherwise. As the system studied is isotropic, the formula can be converted to a one-dimensional correlation function *S(r)* depending only on the distance *r*.

$$S(r) = \frac{1}{2r+1} \sum_{l=0}^{2r} S(r, \frac{\pi l}{4r}).$$

For comparison, results are presented in terms of the normalized two-point correlation functions, to eliminate the minor influence of variable volumetric phase fractions between model and real microstructure images. The normalized two-point correlation function is calculated as:

$$N(r) = \frac{(S(r) - S(0) \times S(0))}{(S(0) - S(0) \times S(0))},$$

where $S(0)$ represents the volume fraction of the phase of interest. In this case, $S(0)$ is the average density of pits in the image.
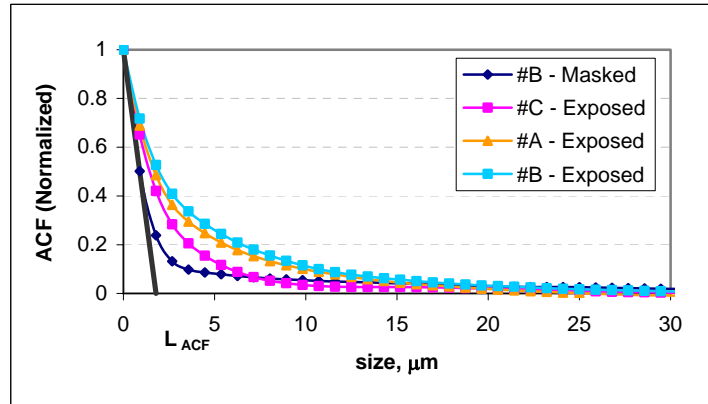

Figure 15. ACF of the four pit threshold images from Figure 13.

A characteristic length of the ACF function, $\mathbf{L}_{ACF}$, is defined as the intersection of the x-axis and the tangent to the ACF autocorrelation function curve at x=0. Results for $\mathbf{L}_{ACF}$ and S(0) are shown in Table V. The results for the autocorrelation function follow the same trends as the fast Fourier transform (FFT) analysis, with the higher $\mathbf{L}_{ACF}$ value

reflecting a larger average size of the dark domains (pits) in the images. In general, for coatings with pits, we expect that the gloss will depend on RMS roughness, L_{ACF} and S(0).

Table V. Characteristic length and density of pits from ACF for the four threshold images and the corresponding RMS roughness, and 60° gloss values.

	#B-Masked	#C-Exposed	#A-Exposed	#B-Exposed
S(0) (area fraction of pits)	0.027	0.223	0.276	0.297
Characteristic Length L_{ACF} , μm (±3%)	1.67	2.50	2.76	3.08
RMS, μm-LSCM 150x (±0.05μm)	0.10	0.22	0.27	0.27
60° gloss (±1)	55	30	21	23

Preliminary Studies of the light scattering angular distribution
As the above discussion makes clear, it is possible to use LSCM to accurately characterize the distribution of important topographical components of the coating surface. Moreover, from the theory of gloss, it is expected that for the most part, these components, such as near-surface pigments and surface pits or depressions, will act as independent diffuse scatterers of the incident light. To fully link gloss changes to the surface morphology changes resulting from weathering, an analysis of the non-specular diffuse light scattering distribution becomes vital.

We are now beginning such light scattering studies. Figure 16 shows scattering distributions for panels #A, #B and #C at the $(60^o, - 60^o)$ scattering configuration (at incident angle, $\theta_o = 60^o$ and detection angle, $\theta_s = -60^o$). It may be observed that the angular spread and shape of the intensity distribution is different for the three coatings, with a narrower angular spread for panel #B, and for each coating, less near-specular scattered intensity for the lower gloss exposed area.

Using a short exposure time to avoid detector saturation, the total scattered intensity was calculated for the $60^o \pm 0.9°$ detection angle range, corresponding to the gloss meter collection angle. The results, shown in Table VI, show a general trend consistent with the gloss measurements, but the two quantities are not strictly proportional. The reasons for this discrepancy might be due to factors such as the difference in incident light source (single wavelength vs. continuous spectrum), light absorption effects from the pigment, and differences between the two methods in the collecting geometry and the size of the sample area.
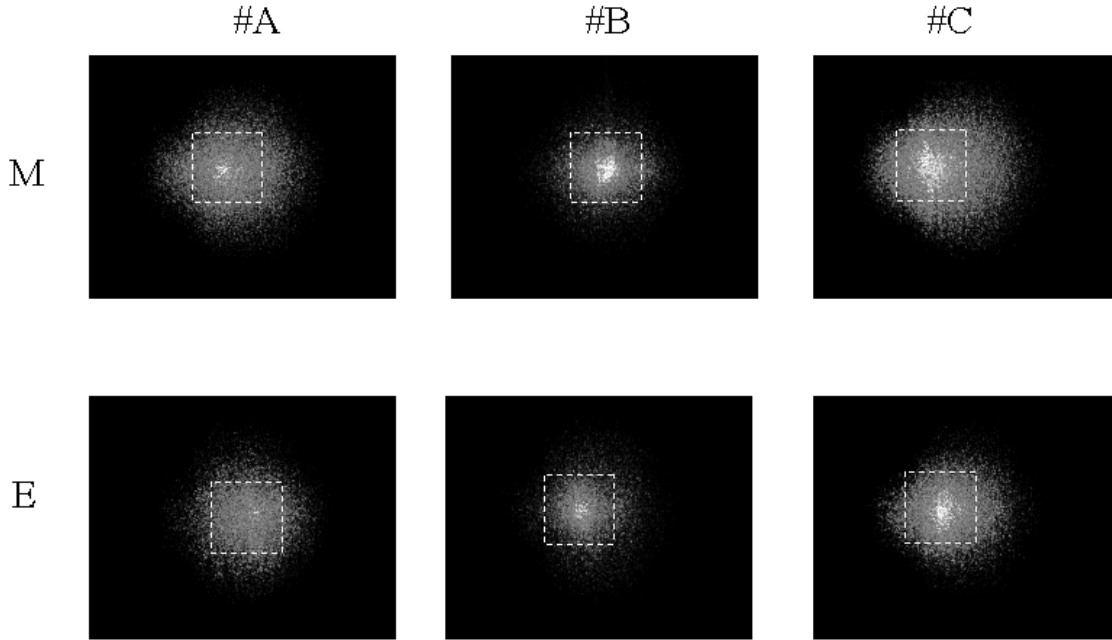
Figure 16: Light scattering profiles (two-dimensional (2D) image) were measured from the masked (M) and exposed (E) surfaces of three samples #A, #B, and #C at (60°, -60°) (i.e. θ_o =60° & θ_s = -60°) scattering configuration. The exposure time of the 2D detector is 0.125 s. Each 2D image consists of 1300 pixels x 1030 pixels and 140 pixels per degree. The central box indicates an angular region of +/- 0.9° from specular angle.

Table VI. List of 60° gloss values, RMS roughness values from LSCM-150x, and the corresponding total light intensity obtained from light scattering measurement for the masked and unmasked areas of samples #A, #B, and #C. Here, total light intensity was obtained by integrating the scattered light intensity (exposure time = 0.03125s) within the angular range +/- 0.9° from specular angle.

		60° gloss (±1)	RMS, µm LSCM 150x (±0.05 µm)	Total light intensity in the central region ($\times 10^{-6}$ count, ± 4%)
Masked	**#A**	48	0.15	5.16
	#B	55	0.10	5.34
	#C	57	0.10	5.53
Exposed	**#A**	21	0.27	4.08
	#B	23	0.27	3.88
	#C	30	0.22	4.17

The off-specular scattering portion— more than ± 0.9° off of the specular reflection angle—is not collected in a typical 60° gloss measurement. The scattering intensity profile in this region can provide information about the roughness at a shorter wavelength scale, including information about the scattering from pigment particles. Figure 17 shows

the scattering profiles for sample #B over the $(60^o, -57^o)$ cattering angle range. Again, less near-specular scattered intensity is observed for the lower gloss exposed area of the test panel, but more off-specular diffuse scattering. We are now conducting light scattering experiments to fully measure the off-specular scattering profiles.
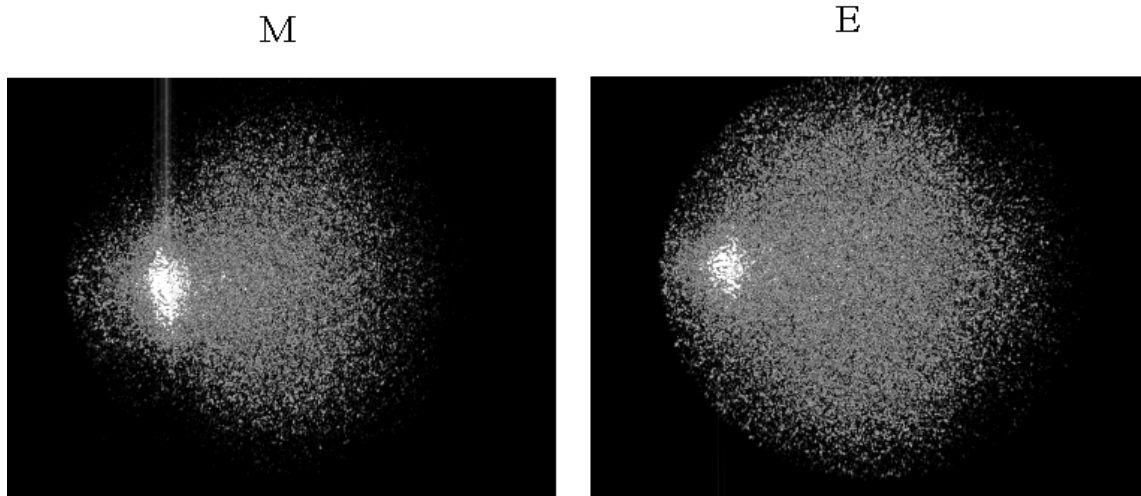
M E

Figure 17: Light scattering profiles were measured from the masked (M) and exposed (E) surfaces for sample #B at (60°, -57°) (off-specular) scattering configuration. The exposure time of the 2D detector is 0.5 s.

Conclusions

We have investigated the relationship between the gloss loss and the change in surface morphology for PVDF paints weathered for 10 years in Florida using Laser Scanning Confocal Microscopy (LSCM). Paints made with different pigment grades showed different degradation characteristics after exposure. Changes in gloss have been correlated with surface roughness and other topographical features including the formation of micron-scale pits and the distribution of pigment particles at the surface.

For PVDF coatings exhibiting pits, the increase in RMS surface roughness, and the decrease in the coating gloss after exposure, appear to be dominated by the formation of pits, rather than by the emergence of pigment particles at the coating surface. To our knowledge, this is the first time that pits of these dimensions have been implicated as the principal proximal cause of gloss changes in some pigmented coatings. Most theoretical predictions[6,7] focus instead on the role of emerging pigment particles at the coating surface.

For a relatively large sample set, a linear relation was found between the 60° gloss and the RMS roughness measured using the LSCM at a low (5x) magnification (10 μm to1000 μm length scale). At higher magnification (smaller length scales), a similar trend exists, but with a lower degree of statistical correlation. Moreover, a scaling relationship was found between the local RMS roughness value and the corresponding measured

length scale. This result implies that each coating surface has an intrinsic fractal surface dimension, implying that fractal analysis may potentially provide a link between physical changes at the nanoscale and macroscale levels, which could be used in service life predictions of gloss retention.

Many of the weathered samples have prominent micron-scale pits or depressions on the surface. For a number of samples displaying pits after weathering, the histograms of scattered light intensity for unexposed (masked) and exposed areas of the paints reveal a minimal increase in the density of pigment particles at the top surface due to weathering. Using the intensity histograms, criteria can be established to generate binary images of the pits and the surface pigments. These images were analyzed using the Fast Fourier Transform (FFT) and Autocorrelation Function (ACF) techniques. The techniques generate characteristic lengths (L_{FFT}, L_{ACF}) which can be used to quantify weathering-induced changes in the local surface morphology. For both techniques, the characteristic lengths determined from binary images of the pits, especially at high magnification, show a good correlation with macroscopic gloss measurements (the larger the characteristic length of the pit spatial distribution, the lower the gloss values).

To attempt to establish a more quantitative link between the scattering of surface topographical features with the measured coating gloss, we are initiating studies to look at the full angular distribution of scattered light from the coatings, using a new light scattering apparatus developed at NIST. In addition to these studies of the relation of the coating topography to the gloss, mechanistic studies of the coating degradation are underway using the 2-meter-Integrating Sphere[20] developed by NIST, as well as other kinds of accelerated test cabinets.

References

1 Iezzi, R.A., "Fluoropolymer coatings for architectural application, "*Modern Fluoropolymers*; John Wiley & Sons Ed., Chap. 14, 271 (1997).

2 See for instance Nguyen, T. et al., "Relating laboratory and Outdoor Exposure of coatings: II. Effect of relative Humidity on photodegradation and the apparent Quantum Yield of acrylic-Melamine Coatings" *J. Coatings Technology,* Vol. 74 (932), 65 (2002) and a number of articles in Bauer, D.R.; Martin, J.W. eds. "Service Life Prediction: Methodology and Metrologies" *ACS Symposium,* Series 805 (2002).

3 Wood, K.A.; Cypcar, C.; Hedhli, L., "Predicting the exterior durability of new fluoropolymer coatings," *J Fluorine Chemistry*, 104, 63 (2004).

4 Corle, T.R.; Kino, G.S., "Confocal Scanning Optical Microscopy and Related Imaging Systems," pp 37-39 (Academic Press 1996).

5 Sung, L.P.; Garver, J., Embree, E., Dickens, B.; Martin, J.W., "A novel light scattering instrument for characterizing polymeric coating materials," to be published.

6   Colling, J. H.; Dunderdale, J., "The Durability of Paint Films Containing Titanium Dioxide—Contraction, Erosion and Clear Layer Theories," *Prog. Org. Coat.,* 9, 47 (1981).

7   Braun, J.H., "Titanium Dioxide's Contribution to the Durability of Paint Films", *Prog. Org. Coat.* 15, 249 (1987).

8   VanLandingham, M.R.; Nguyen, T.; Byrd, W.E.; Martin, J.W. "On the Use of the Atomic Force Microscope to Monitor Physical Degradation of Polymeric Coating Surfaces:, *J. Coatings Technology* 73 (923), 43 (2001).

9   Nguyen, T.; Gu, X.; VanLandingham, M.R.; Byrd, W.E.; Martin D.; Ryntz, R.; Martin, J.W. " Degradation Modes of Polymeric Coatings exposed to UV," *Proceedings of the 7th International Coatings for Plastics Symposium (Troy, MI, June 2004).*

10 Faucheu, J.; Wood, K. A. *Proceedings of 3rd International Symposium on Service Life Prediction of Coatings (Sedona AZ, February 2004).*

11 Biggs, S.; Lukey, C.A.; Spinks, G. M.; Yau, S.-T., "An Atomic Force Microscopy Study of Weathering of Polyester/Melamine Paint Surfaces," *Prog. Org. Coatings* 42, 49 (2001).

12 Wood, K.A.; Hedhli L.; Willcox, P.J., "Patterns of Erosion from Acrylic and Fluoropolymer Coatings in Accelerated and Natural Weathering Tests," *J. Coatings Technology*, 74 (924), 63 (2002).

13 Gu, X.; Sung, L.; Ho, D.L.; Michaels, C.A.; Nguyen, D.; Jean, Y.C. and Nguyen, T., "Surface and Interface Properties of PVDF/Acrylic Copolymer Blends Before and After UV exposure**,"** *FSCT·ICE 2002 Proceedings of the 80th Annual Meeting Technical Program*, Oct. 30 – Nov 1, New Orleans, LA. (2002).

14 Alexander-Katz, R.; Barrera, R.G., "Surface Correlation Effects on Gloss," *Journal of Polymer Science: part B: Polymer Physics,* Vol. 36, 1321 (1998).

15 Whitehouse, D.J.; Bowen, D.K.; Venkatesh, V.C.; Lonardo, P.; Brown, C.A., "Gloss and Surface Topography," *Annals of the CIRP,* Vol. 43, 541 (1994).

16 Assender, H.; Bliznyuk, V.; Porfyrakis, K., "How Surface Topography Relates to Materials' Properties," *Science* Vol. 297, 973 (2002).

17 Johnson, M. A. and Cote, P. J., "Detrended Fluctuation Analysis of UV Degradation in a Polyurethane Coatings," *J. Coatings Technolog*y**,** 75, No. 941, 51 (2003).

18 Ginneken B. V., Stavridi M, Koenderink J.J., "Diffuse and Specular Reflectance from Rough Surface," *Applied Optics* 37, 1, p130 (1998)

19 Bentz, D.P., "Quantitative Comparison of Real CEMHYD3D Model Microstructures Using Correlation Functions," *submitted to Cement and Concrete Research* (2004).

20 The current output at each port of the 2-meter-Integrating SPHERE is about 22 "sun" -Intensity of 1 "Sun" is equal to 22 W/m^2 (ASTM E891) and is rich in the region between 290 nm and 400 nm. For technical information: Chin J.W., Byrd E., Embree N., Martin J., Tate J.D. "Ultraviolet Chambers Based on Integrating Spheres for Use in Artificial Weathering" *J. Coatings Technology, 74 (929),* 39 (2002)**.**